An in Situ Study of Precursor Decomposition via Refractive Index Sensing in p-Type Transparent Copper Chromium Oxide

(article starts on next page)

An *In Situ* Study of Precursor Decomposition via Refractive Index Sensing in p-Type Transparent Copper Chromium Oxide

Ainur Zhussupbekova,* Kuanysh Zhussupbekov, Ruggero Verre, David Caffrey, Kyle Shiel, Igor V. Shvets, and Karsten Fleischer

ACCESS | Metrics & More | Article Recommendations | Supporting Information

ABSTRACT: Oxide semiconductors are penetrating into a wide range of energy, environmental, and electronic applications, possessing a potential to outrun currently employed semiconductors. However, an insufficient development of p-type oxides is a major obstacle against complete oxide electronics. Quite often oxide deposition is performed by the spray pyrolysis method, inexpensive to implement and therefore accessible to a large number of laboratories. Although, the complex growth chemistry and a lack of *in situ* monitoring during the synthesis process can complicate the growth optimization of multicomponent oxides. Here we present a concept of plasmonic, optical sensing that has been applied to spray pyrolysis oxide film growth monitoring for the first time. The proposed method utilizes a polarization based refractive index sensing platform using Au nanodimers as transducing elements. As a proof of concept, the changes in the refractive index of the grown film were extracted from individual $Cu(acac)_2$ and $Cr(acac)_3$ precursors in real time to reveal their thermal decomposition processes. Obtained activation energies give insight into the physical origin of the narrow temperature window for the synthesis of high performing p-type transparent conducting copper chromium oxide Cu_xCrO_2. The versatility of the proposed method makes it effective in the growth rate monitoring of various oxides, exploring new candidate materials and optimizing the synthesis conditions for acquisition of high performing oxides synthesized by a high throughput cost-effective method.
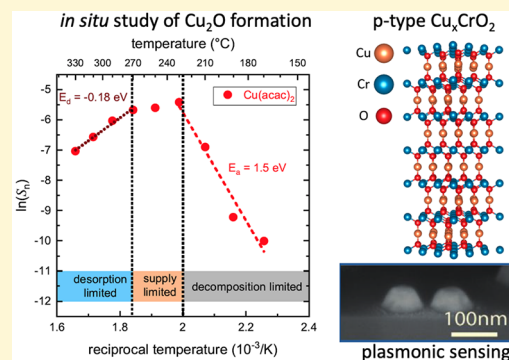
INTRODUCTION

Transparent conducting oxides (TCOs) are materials possessing a rare combination of two contradicting properties of electrical conductivity and optical transparency in a single material. Exhibiting this remarkable coexistence of properties, TCOs are desired materials in a broad range of applications including solar cells, flat panel displays, touch screens, light emitting diodes, transparent electronics, memristors, and neuromorphic applications

The most common and better performing TCOs are n-type, while the development of high performing p-type TCOs remains an outstanding challenge due to low hole density, localized nature of the valence band derived of O 2p, and large hole effective masses.[1,2] Despite current limitations, p-type TCOs have been already used to selectively extract and transport p-type charge carriers[3] in thin film solar cells[4,5] and organic light emitting diodes and have been also used as a UV-blocking layer to improve the photostability of dye sensitized and perovskite solar cells.[6] These applications are a consequence of the wide band gap of p-type TCOs, their thermal stability, a high work function, and good hole conductivity.[7] To best serve these technologies, p-type TCOs have to display an appropriate valence band structure, well aligned with the high work function of a contact and the

valence band[8] of the photoactive layer to effectively suppress diffusion between the electrode material and the photoactive layer.

A class of p-type TCO material with the potential to solve the issue of low performance is copper-based delafossite oxides with a general formula $CuMO_2$ in which M corresponds to a trivalent cation such B, Al, Cr, Ga, Sn In, or Y. The delafossite structure is composed of each Cu atom linearly coordinated with two O atoms, forming an O−Cu−O dumbbell parallel to the *c*-axis. Every oxygen anion is also coordinated to M^{3+} cations oriented in a way that the M-centered octahedra form MO_2 layers that are parallel to the *ab* plane.[1] Usually Cu-based delafossites have higher conductivity values yet lower Hall mobility values.[9] This higher conductivity is possibly justified by the hole concentrations produced by a higher density of native acceptor-like defects.[1] One notable exception within the class of copper delafossites is $CuCrO_2$,[10] where the top of the
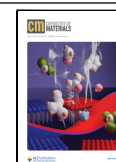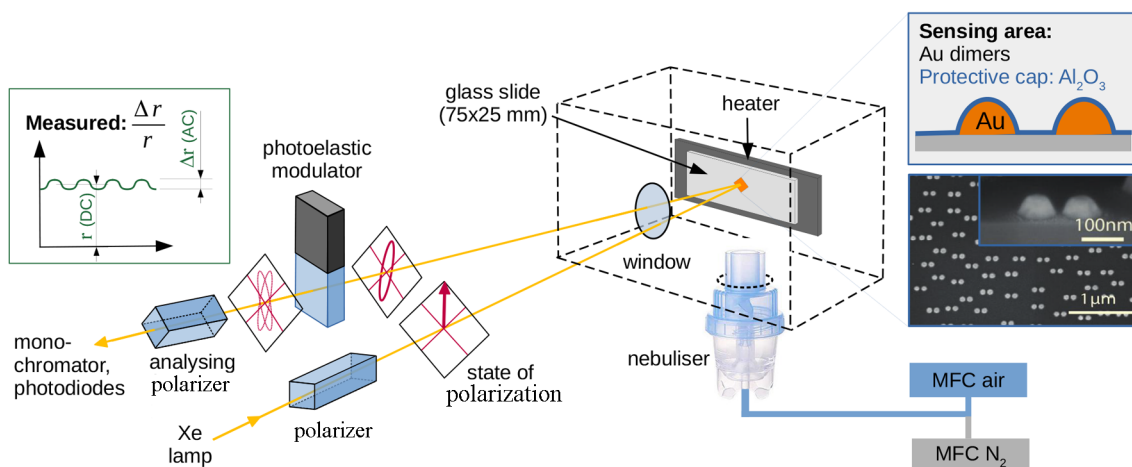
Figure 1. Schematic of the small spray pyrolysis chamber and the main optical components of the RAS setup. The inset shows the SEM image of Au dimers before Al_2O_3 capping.

valence band was found to be formed by the Cr 3d states rather than the Cu 3d state.[11−13] This facilitates an insensitivity to the crystalline quality as the conduction is based on a hopping mechanism between CrO_2 octahedra, allowing for nanocrystalline or even amorphous p-type TCOs grown at much lower temperatures than conventional copper delafossites.

Previously a very narrow processing window for spray pyrolysis grown, best performing p-type Cu_xCrO_2[14,15] was reported. In order to analyze the origin of this narrow temperature window for Cu_xCrO_2 synthesis, a concept of plasmonic, optical sensing is applied to spray pyrolysis for the first time, allowing *in situ* oxide film growth monitoring by probing of the activation energies of the film formation process. The gradual changes of the effective medium between the Au nanoparticles from air to Cu_xCrO_2 during film formation were monitored using a polarization-based *in situ* optical sensing technique for a variety of growth temperatures. This methodology was tested using two widely employed[16] $Cu(acac)_2$ and $Cr(acac)_3$ precursors, yet the versatility of the technique allows for it to be applied to real time growth monitoring of various oxides. To further explore the tunability of Cu_xCrO_2 films, the influence of temperature and oxygen partial pressure on the film composition and electrical performance was investigated.

■ METHODS

Gold Nanoparticles Preparation. The Au dimers are made by hole−mask colloidal lithography.[17] To investigate the spray pyrolysis process, substrate temperatures of up to 400 °C are required. To minimize any changes in the Au-dimer shape and size, during the actual measurements all Au-dimer substrates are pretreated by coating with a 2 nm thin Al_2O_3 film grown by atomic layer deposition (Oxford Instruments, 250 °C, 20 cycles of 20 ms pulse of TMA precursor, each followed by Ar purge and water pulse). Fuctionalized substrates were preheated to 400 °C prior to material deposition and optical sensing.

Spray Pyrolysis Using Medical Nebulizers. p-Type Cu_xCrO_2 oxide films were deposited on standard microscope glass slides (Thermo Scientific 2.5 × 5 cm, 1 mm thick) by spray pyrolysis. In contrast with the commonly employed air-blast nozzle modified setup, we employ a medical grade nebulizer positioned in a small chamber with an optical window, used for *in situ* monitoring. The same pyrolytic decomposition of the dissolved precursors, sprayed by the stream of carrier gas toward the surface of a substrate, governs the

deposition. In contrast to conventional spray pyrolysis, the different nebulization method of the solution allows the formation of high-quality, smooth films at lower substrate temperatures. In a conventional spray pyrolysis system, MAD-0331-B1B Ultrasonic Atomisers were employed; they tend to produce a broad range of droplet sizes ranging from ≈10−30 μm.[18] The average droplet sizes produced by mist chemical vapour deposition (CVD) are found to be around 5.4 μm.[19] The main difference is a reduction in the active cooling from the nebulizing gas, as much lower gas flow rates are required. In addition, the more homogeneous droplet size distribution and the reduced impact damage from larger droplets accelerated onto the film by the high pressure in air blast nebulizers further improve the film morphology.

The liquid precursor solution was prepared by dissolving $Cu(acac)_2$ and $Cr(acac)_3$ in methanol with a 70:30 Cr/Cu ratio, an overall total molarity of 0.03 M,[20] and a gas flow of 4 L/m. The choice of precursors is based on characteristics such as volatility, thermal stability, and reactivity.[21,22] The solution was nebulized by a Hudson RCI Micro Mist nebulizer creating a "mist", which is transported toward the heated substrate (Watlow CER-1-01-00250 Ultramic ceramic heater). The temperature triggers the evaporation of the solvent while vaporized precursors remain in a gaseous state to form a desired material on the substrate surface.[23] A range of processing temperatures were tested, and the optimum temperature for good conductive Cu_xCrO_2 was found to be 310 °C, approximately 40 °C lower than in our conventional air-blast nebulizer system using the same precursors.[14,15]

The precursor activation energy study was conducted in the same chamber, as it is equipped with a window for *in situ* optical sensing. Each precursor was studied separately in the temperature range from 230 to 390 °C. The film formation was monitored by observing changes in the localized surface plasmon resonance (LSPR) of anisotropic gold dimers.[24]

X-ray Photoelectron Spectroscopy. The film composition was measured by X-ray photoelectron spectroscopy (XPS) in an Omicron MultiProbe XPS using a monochromized Al Kα source (XM 1000, $E_{h\nu}$ = 1486.7 eV). Prior to XPS measurements films were sonicated in acetone and isopropanol for 10 min and then etched via an argon ion gun operated at a low voltage of 750 eV with a sputter current of ≈6 μA and chamber pressure of 1.5 × 10^{-3} Pa to ensure removal of unreacted precursors. Representative XPS scans are shown in the Supporting Information (SI).

Raman Spectroscopy. Raman spectra of Cu_xCrO_2 samples were recorded using a JY Horiba LabRAM800 confocal micro-Raman setup with motorized positioning stages. The excitation wavelength was 488 nm, power ∼ 10 mW, and the integration time was 5 min. To maximize the Raman signal from the thin films, the underlying

substrate was numerically subtracted for each spectrum. Details of the subtraction method were previously reported.[25]

Optical Characterization. Optical properties were measured via UV−visible spectrophotometry (UV−vis) on a PerkinElmer S650 instrument.

Electrical Properties. The carrier activation energy is determined from the four point linear probe measurements using a Keithley 2400 source meter. Seebeck measurements were performed as previously described[13] (see SI).

Thickness Measurements and Modeling. The thickness of each film was determined by X-ray reflection (XRR) (Bruker D8-Discover) as well as by optical modeling of UV−vis transmission and reflectance spectra. By dividing the film thickness with the growth time, the average growth rate for each film was determined in absolute terms of nm/min.

■ RESULTS AND DISCUSSION

Methodology of *In Situ* Spray Pyrolysis Growth Monitoring. The synthesis of any ternary material is a complex process. The possibility of monitoring the properties of the films *in situ*, during the growth, enables the determination of vital information, such as the refractive index of the material and the growth mechanisms. For this reason, reflectance based optical techniques are frequently employed.[26−29] However, in the spray pyrolysis the nebulized solution generates large scattering and droplet absorption along the light path within the chamber, rendering standard intensity-based reflectance measurements challenging.

In order to allow *in situ* measurements of the spray pyrolysis process, a sensing approach based on polarization based refractive index sensing was adapted.[24] Previously, the method was used for optical biosensing that allowed the analyzation of molecular interactions at the nanoscale. However, the usage of plasmonic nanoparticles for oxide growth sensing has never been performed before. Therefore, a small deposition chamber was specifically designed with an optical window normal to the sample surface as schematically demonstrated in Figure 1. The sample was clamped on a vertically mounted heater with the nebulizer placed directly underneath, allowing the use of low cost medical nebulizers. The gas supply was controlled by mass flow controllers (MFCs) to allow for a controlled variation of the oxygen partial pressure, as well as reproducible gas flow rates into the nebulizer. The entire setup was mounted on an optical alignment stage allowing for adjustment of the reflected beam more precisely. The material was deposited on a glass slide with 10% surface area covered by plasmonic Au nanodimers, all aligned along the same direction. An electron micrograph of a typical surface is shown in the inset in Figure 1. The morphological anisotropy of the plasmonic nanostructure induces an optical anisotropy in the glass substrate, as the light is absorbed differently along and perpendicular to the dimer axis. When linearly polarized light is sent at a normal incidence of 45°, rotated with respect to the dimer axis, the optical anisotropy causes a rotation of the polarization axis of the reflected beam. If light is sent at a normal incidence, the rotation angle of light is proportional to the reflectance anisotropy of the surface using the small angle approximation $\sin \theta = \theta$

$$\theta = \frac{1}{2} \times \frac{\Delta r}{r}$$

where r is the complex reflectance of the sample along the ith direction; $\frac{\Delta r}{r}$ is also known as reflection anisotropy spectros-

copy (RAS), and it is a self-normalized quantity that monitors the relative change in intensity between two orthogonal directions. Details and the specific use in refractive index sensing are found elsewhere.[24,30,31]

The strong RAS signal from Au dimers arises from a difference in polarizability along and perpendicular to dimers direction as is schematically demonstrated in Figure 2a.
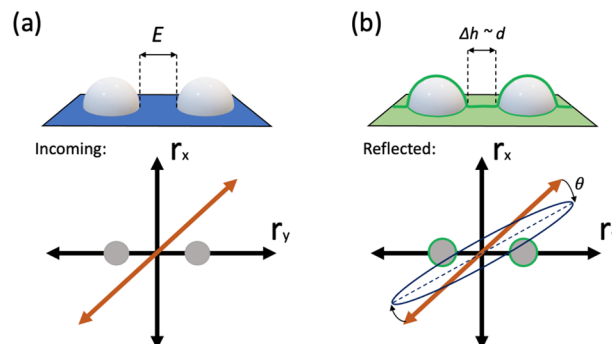

Figure 2. RAS signal acquisition from gold dimers (a) before deposition and (b) after deposition.

Therefore, the Au nanodimers act as local optical transducers retrieving the optical properties of the TCO growth *in situ*. In fact, not only do the Au dimers induce a rotation of the polarization angle of the polarized light, but they are extremely sensitive to their surrounding refractive index (n) and the thickness (d) of the deposited film as is shown in Figure 2b. The plasmonic nanostructure can be used to extract indirect information on the spray pyrolysis film characteristics. Increasing the refractive index between the nanoparticles in a subsequent growth run will, in a first order approximation, shift the plasmonic resonance toward the infrared due to an increase of the effective medium surrounding the Au nanoparticles.

To allow for a simple comparison between different spectra, the transient of RAS as a function of time is monitored in the region of largest sensitivity of the spectra, at 1.85 eV (see SI for details on the normalization procedure). Due to the self-normalizing nature of the RAS measurement, variations in total intensity caused by fluctuations and turbulence in the nebulizer mist do not effect the spectra. In principle, the setup also allows for measurements of the total reflectance, yet increased noise levels due to the mentioned fluctuations in the droplets around the sample, as well as condensation of unreacted precursor on the inside of the window, limits the use in the simple reflectance mode.

Figure 3 shows a RAS spectrum of a stabilized localized surface plasmon resonance (LSPR) of an anisotropic gold dimer meta-surface acquired before and after a deposition step S_{spec} (a), as well as a transient S_{trans} (b) during the deposition. The rise in the RAS signal during the transient measurement shows an increase in material deposited over and between the gold dimers. Normalization of the latter with the spectral slope provides a renormalized value $S_n = S_{trans}/S_{spec}$ that is proportional to the product of the film growth rate and refractive index, measured for the temperature and precursor combination chosen for investigation. For ultrathin films, all optical methods are only sensitive to the product of the refractive index and thickness ($n \times d$) due to the fundamental nature of light interaction at interfaces.[32,33]
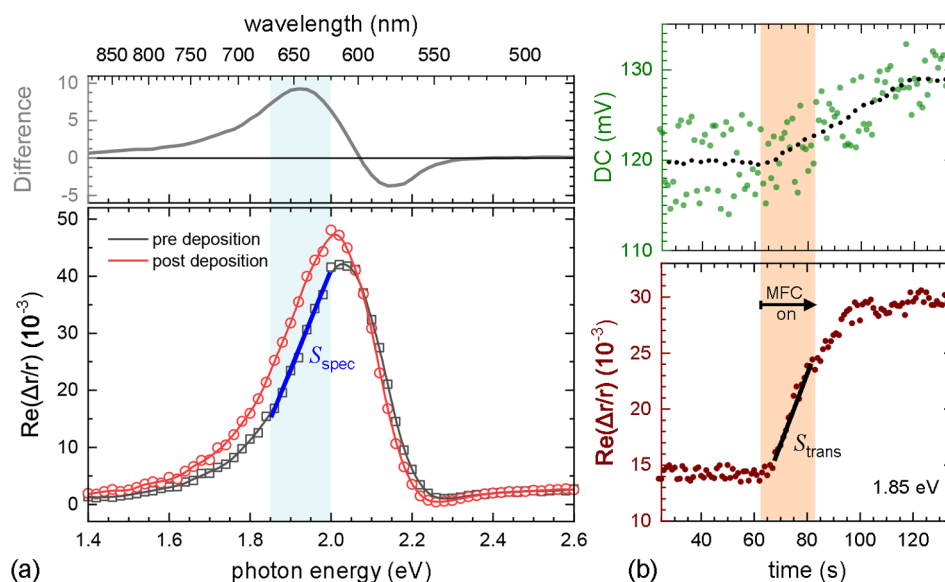
Figure 3. Example of a deposition cycle. (a) RAS spectra of the LSPR meta-surface at 230 °C before and after a deposition cycle using a 0.01 M solution of $Cu(acac)_2$ in methanol. The top panel shows the difference in the two spectra. The shift in the spectral position of the plasmon resonance is evident. In the shaded regions there is a large difference and a nearly linear spectral dependence. Single wavelength, transient measurements during depositions are best taken there. (b) Transient measurement at 1.85 eV taken during growth. The shaded area indicates the time when the gas supply to the nebulizer was on. The top panel shows the DC level of the measurement proportional to the intensity of the reflected light.
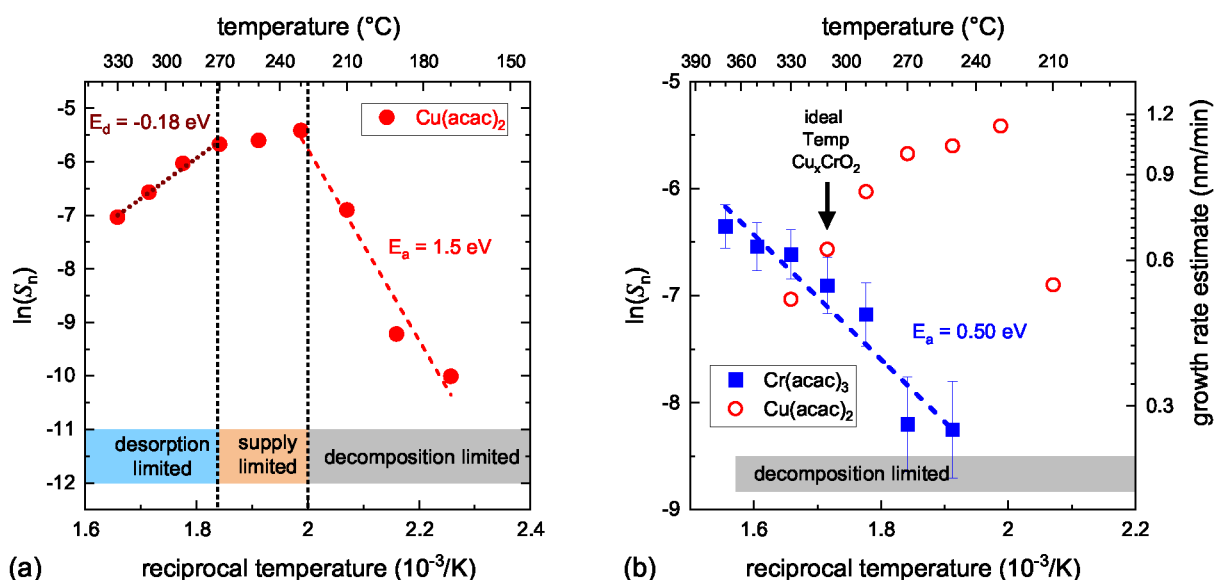

Figure 4. Arrhenius type plots of the normalized slope S_n for (a) the $Cu(acac)_2$ precursor (0.01 M solution). (b) Comparison of the $Cr(acac)_3$ precursor (0.015 M solution) measurement to those of $Cu(acac)_2$. Both measurements were performed with 5% oxygen content in the nebulizing gas. The estimated growth rate scale in (b) is given as a rough guide and is based on an assumed linear relationship of the growth rate with molarity and S_n.

For our analysis we assume that n does not significantly vary for the material formed at the different temperatures. While this is a simplification, and the refractive index of the material may easily vary by 10% within the first 2−10 nm,[34,35] a change in thickness from 1 to 2 nm changed d by 100%. Hence the thickness change will dominate the response. Therefore, our methodology is beneficial in an optimization and fast screening of the synthesis of novel multicomponent oxides as well as in understanding the growth mechanism and chemistry of the spray pyrolysis process.

Precursor Decomposition Screening for Copper Chromium Oxide. Thermal decomposition studies of acetylacetonate precursors have found that the $Cu(acac)_2$ precursor starts to decompose at 200 °C while the corresponding $Cr(acac)_3$ starts to decompose at 250 °C.[36] More recent work has shown that the $Cr(acac)_3$ precursor will have lost at least one (acac) group at 280 °C.[37] However, the precursor decomposition is only the first step in the spray pyrolysis growth process. It then also involves subsequent adsorption of the precursor onto the surface, either in an
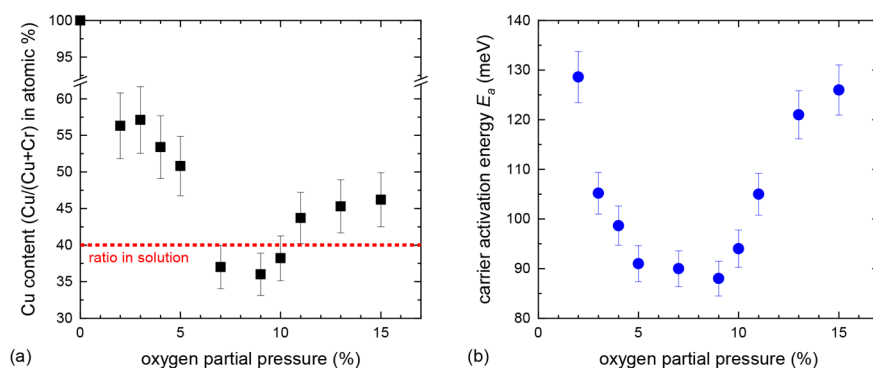
Figure 5. Film composition (a) and carrier activation energy (b) as a function of oxygen content in the nebulizing gas. Each sample was deposited until the full cup of 8 mL is emptied at a temperature of 310 °C.

unreacted form or in a partially decomposed form. The adsorption itself will depend on the surface termination and temperature. Indeed, it is already known that $Cr(acac)_3$ adsorption can be self-limited, preventing a continuous growth at low temperatures. Due to these properties, $Cr(acac)_3$ is used as an atomic layer deposition precursor, where this self-limitation is employed and Cr_2O_3 is formed with subsequent oxidation steps.[38] In spray pyrolysis the presence of oxygen in the chamber, as well as OH groups and H_2O from the further pyrolytic decomposition of the precursors and solvents, can lead to continuous reactions and film formation.

By probing the buildup of the fully formed oxide layer around the plasmonic nanoparticles, it is possible to examine the thermodynamics of the entire spray pyrolysis process. As discussed above, one can determine a normalized slope S_n for each precursor and temperature. Plotting $\log(S_n)$ in an Arrhenius type graph vs $1/T$ shows characteristic differences between the Cr and Cu precursors that are depicted in Figure 4.

As expected from the thermal decomposition studies, the Cu precursor is more reactive at lower temperatures than the Cr precursor. For the Cr precursor a linear slope is seen, giving an effective activation energy for the Cr_2O_3 film formation of 0.5 eV. The Cu precursor, in contrast, displays a more complex behavior. At low temperatures the onset of growth is observed, limited by the actual decomposition of the precursor with an activation energy of 1.5 eV. Once the precursor fully decomposes, the kinetically limited regime is reached, where the growth rate depends on the solution molarity and oxygen supply. Increasing the temperature further actually reduces the growth rate significantly. This is characterized by an activation energy for desorption of 0.18 eV. Either the copper suboxides thermally desorb, there is a depletion of the precursor in the gas phase, or the formation of acetic acid in the precursor decomposition at higher temperatures[36] leads to an active etching of the formed Cu_2O.[39]

The observed behavior for the decomposition and oxide film formation for the individual Cu and Cr precursors now directly explains the narrow growth window for Cu_xCrO_2. For temperatures lower than the optimum 310 °C, the Cr precursor does not sufficiently decompose and only Cu_2O is formed independently of the actual Cu molarity in the solution. Increasing the temperature reduces the Cu incorporation dramatically either by Cu suboxide desorption or by depletion of the precursor in the gas phase (see Figure 4a), while also significantly increasing the Cr incorporation. In order to enlarge the temperature processing window for low

cost spray pyrolysis of this specific material, one would need to find a Cr precursor that decomposes more readily at lower temperatures.

Our findings demonstrate that Cr_2O_3 is only formed substantially above 330 °C, yet the ideal growth temperature for the ternary Cu_xCrO_2 is 310 °C. The low temperature regime (<330 °C) is also likely to be dominated by the adsorption of unreacted $Cr(acac)_3$ rather than actual Cr_2O_3 formation. We observe no film growth in this range when using higher molarity solutions, in line with self-limited adsorption[38] Therefore, the presence of Cu suboxides must alter the $Cr(acac)_3$ adsorption or on-surface decomposition. In mixed solutions, the *in situ* optical monitoring is of less use, as it does not distinguish compositions of the growing film. Therefore, to confirm these findings, thicker samples grown for a longer time of 10 min and higher molarity of 0.03 M at 310 °C were considered. The resulting film thicknesses were measured to determine the overall growth rate. Using solutions of 0.03 M $Cu(acac)_2$, the growth rate of 1.5 ± 0.3 nm/min for binary Cu_2O was obtained. The growth rate for a corresponding Cr_2O_3 film using 0.03 M $Cr(acac)_3$ is found to be lower at 0.8 ± 0.2 nm/min. The ratio of 1.8 ± 0.4 between these growth rates is in agreement with the estimation from the *in situ* study where a ratio of 2 was expected based on the values of S_n at 310 °C. Films grown with a *mixture* of $Cu(acac)_2$ and $Cr(acac)_3$ (ratio 40/60), while keeping the total molarity at 0.03 M, have a significantly higher growth rate of 2.4 ± 0.4 nm/min. Clearly the presence of Cu suboxides on the surface dramatically increases the Cr incorporation at this temperature, and such an effect has been seen for other ternary oxide growth.[40,41] Indeed the film is almost twice thicker than expected for a pure linear combination of the Cu_2O and Cr_2O_3 growth rate.

Tunability of Copper Chromium Oxide via Oxygen Partial Pressure. To further explore the possibilities of Cu_xCrO_2 tuning, an in-depth analysis of the oxygen role in the film formation was conducted. Figure 5a shows the stoichiometry of bulk films grown from the same solution as a function of oxygen partial pressure. Growing in full nitrogen leads to the formation of an insulating Cu_2O film, confirmed via XPS and Raman spectroscopy, while supplying only 2% of oxygen creates the condition for Cu_xCrO_2 formation. Instrumental limitations of the MFCs prevented investigations in the 0−2% range. A further increase in oxygen initially further increases Cr incorporation, and between 5% and 10% oxygen content in the nebulizing gas the film stoichiometry matches the solution stoichiometry. Increasing the oxygen
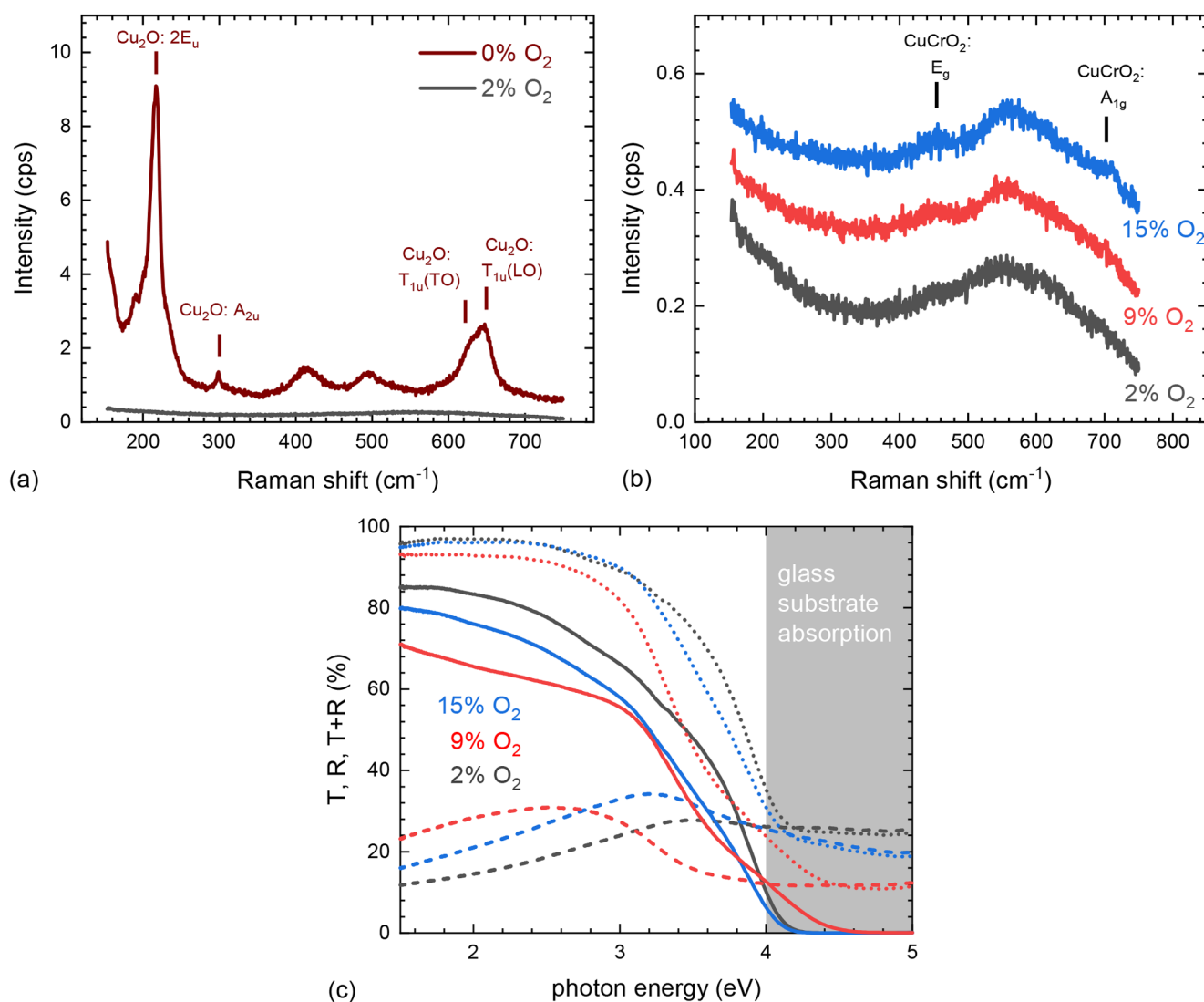
Figure 6. Raman spectra of films grown at varying oxygen content in the nebulizing gas: (a) full nitrogen and 2% oxygen and (b) 2%, 9%, and 15% oxygen. Labels indicate expected peak positions for highly crystalline materials. (c) T (solid lines), R (dashed lines), and $T + R$ (dotted lines) of the same films. Changes are dominated by differences in overall film thickness, with 9% being the thickest.

content above 10% inhibits Cr incorporation again, and at the same time films become more resistive with a noticeable increase in carrier activation energy as seen from Figure 5b.

As temperature and solution stoichiometry remain unchanged, this suggests that the Cr precursor preferentially adsorbs on the Cu−O terminated surface in oxygen poor conditions. Insufficient oxygen supply prevents the adsorption of Cr precursor at 310 °C as seen in the sole formation of Cu_2O in this case. At the same time, an excess of oxygen is detrimental to Cr adsorption as the films get thinner and more Cu rich again (see Figure 5a). This may suggest an overoxidized Cu−O layer possibly creating CuO instead of Cu_2O. Indeed, studies of $Cu(acac)_2$ decomposition in atmospheric CVD reactors have shown CuO formation when a carrier gas mixture of 10% O_2/N_2 has been used, although experiments were done at higher temperatures.[42] Hence, these conditions are likely detrimental to Cu_xCrO_2 formation where Cu is in the same charge state as in Cu_2O. At the same time one also needs to prevent the formation of oxygen vacancies and, as discussed above, oxygen is required for the

incorporation of the Cr. Both effects combined explain the overall dependency of film stoichiometry and film conductivity on the oxygen content. The optimum oxygen content in the nebulizing gas is therefore highly dependent on the instrument, as in larger chambers more residual oxygen in the surrounding atmosphere can influence the growth.

The dramatic change in film composition upon the change of nebulizing gas from full nitrogen to a gas mixture that contains oxygen is most noticeable in the Raman spectra (shown in Figure 6a,b), where for the nitrogen case strong Cu_2O Raman modes are observed, while films containing oxygen only demonstrate very weak and broad modes consistent with the nanocrystalline nature of the Cu_xCrO_2. The expected position for the E_g and A_{1g} Raman modes for crystalline Cu_xCrO_2 are 460 and 710 cm^{-1}, respectively.[43] The increase in oxygen does not change the position yet slightly sharpens the Raman modes, indicating a less defective material. This is consistent with the increased carrier activation energy and higher resistivity of the samples grown in higher oxygen content, as the Cu-vacancy defect structures are crucial for the

conductivity in this material. The Cu_2O Raman spectra of the nitrogen grown sample is dominated by a second-order line at 218 cm^{-1} and the TO and LO phonon modes of a typically Raman inactive mode (T_{1u}). The latter was shown to be increased by point defects, specifically Cu vacancies.[44]

Figure 6c shows transmission (T) and reflection (R) of Cu_xCrO_2 films deposited at various oxygen partial pressures. While we see variation in transmission and reflection, they are largely originating from the changed film thickness rather than substantial changes in the optical properties of the material.

In conclusion, it was demonstrated for the first time that plasmonic sensing is a viable technique for *in situ* growth information acquisition in spray pyrolysis. In particular, refractive index sensing by RAS using plasmonic meta-surfaces to monitor the film growth was performed. Analysis of precursor decomposition and film formation for Cu and Cr precursors allowed the origin of the narrow synthesis window of Cu_xCrO_2 to be identified. Moreover, upon supplying both precursors simultaneously, a Cu induced uptake of Cr incorporation is observed. The produced Cu_xCrO_2 films display low roughness, unusual for inexpensive solution process deposition, confirming that medical grade nebulizers create gentle mist CVD-like growth. The alteration of the oxygen content can be effectively employed to further tune the composition and electrical performance of the films. These results expand the understanding of the synthesis mechanism and doping in ternary copper chromium delafossite. Beyond this specific material, the developed real time growth monitoring method will be applicable for many other spray pyrolysis processes and can quickly identify ideal growth conditions for various ternary oxides or assist in finding alternative precursors to further reduce growth temperatures to minimize the thermal budget of thin film synthesis.

◼ ASSOCIATED CONTENT

Ⓢ Supporting Information

The Supporting Information is available free of charge at https://pubs.acs.org/doi/10.1021/acs.chemmater.1c03910.

> Additional information on the *in situ* optical method employed, as well as measurements and properties of the Cu_xCrO_2 films such as X-ray reflection, details of the electrical characterization, and results (Seebeck, carrier activation energy) as well as representative XPS scans illustrating how the sample stoichiometry was determined (PDF)

◼ AUTHOR INFORMATION

Corresponding Author

Ainur Zhussupbekova − *School of Physics and Centre for Research on Adaptive Nanostructures and Nanodevices (CRANN), Trinity College Dublin, Dublin 2, Ireland;* ⓞ orcid.org/0000-0003-2724-8762; Email: zhussupa@tcd.ie

Authors

Kuanysh Zhussupbekov − *School of Physics and Centre for Research on Adaptive Nanostructures and Nanodevices (CRANN), Trinity College Dublin, Dublin 2, Ireland;* ⓞ orcid.org/0000-0003-1909-3270

Ruggero Verre − *Department of Physics, Chalmers University of Technology, Gothenburg 412 96, Sweden;* ⓞ orcid.org/0000-0001-8337-9009

David Caffrey − *School of Physics and Centre for Research on Adaptive Nanostructures and Nanodevices (CRANN), Trinity College Dublin, Dublin 2, Ireland;* ⓞ orcid.org/0000-0001-7870-4428

Kyle Shiel − *School of Physics, Dublin City University, Dublin 9, Ireland*

Igor V. Shvets − *School of Physics and Centre for Research on Adaptive Nanostructures and Nanodevices (CRANN), Trinity College Dublin, Dublin 2, Ireland*

Karsten Fleischer − *School of Physics, Dublin City University, Dublin 9, Ireland;* ⓞ orcid.org/0000-0002-7638-4480

Complete contact information is available at:
https://pubs.acs.org/10.1021/acs.chemmater.1c03910

Notes

The authors declare no competing financial interest.

◼ REFERENCES

(1) Zhang, K. H.; Xi, K.; Blamire, M. G.; Egdell, R. G. P-type transparent conducting oxides. *J. Phys.: Condens. Matter* **2016**, *28*, 383002.

(2) Youn, Y.; Lee, M.; Kim, D.; Jeong, J. K.; Kang, Y.; Han, S. Large-Scale Computational Identification of p-Type Oxide Semiconductors by Hierarchical Screening. *Chem. Mater.* **2019**, *31*, 5475−5483.

(3) Dunlap-Shohl, W. A.; Daunis, T. B.; Wang, X.; Wang, J.; Zhang, B.; Barrera, D.; Yan, Y.; Hsu, J. W. P.; Mitzi, D. B. Room-temperature fabrication of a delafossite CuCrO2 hole transport layer for perovskite solar cells. *Journal of Materials Chemistry A* **2018**, *6*, 469−477.

(4) Wang, J.; Lee, Y.-J.; Hsu, J. W. P. Sub-10 nm copper chromium oxide nanocrystals as a solution processed p-type hole transport layer for organic photovoltaics. *Journal of Materials Chemistry C* **2016**, *4*, 3607−3613.

(5) Gil, B.; Kim, J.; Yun, A. J.; Park, K.; Cho, J.; Park, M.; Park, B. CuCrO2 Nanoparticles Incorporated into PTAA as a Hole Transport Layer for 85 °C and Light Stabilities in Perovskite Solar Cells. *Nanomaterials* **2020**, *10*, 1669.

(6) Zhang, H.; Wang, H.; Zhu, H.; Chueh, C.-C.; Chen, W.; Yang, S.; Jen, A. K.-Y. Low-Temperature Solution-Processed CuCrO2 Hole-Transporting Layer for Efficient and Photostable Perovskite Solar Cells. *Adv. Energy Mater.* **2018**, *8*, 1702762.

(7) Qin, P.-L.; Lei, H.-W.; Zheng, X.-L.; Liu, Q.; Tao, H.; Yang, G.; Ke, W.-J.; Xiong, L.-B.; Qin, M.-C.; Zhao, X.-Z.; et al. Copper-Doped Chromium Oxide Hole-Transporting Layer for Perovskite Solar Cells: Interface Engineering and Performance Improvement. *Advanced Materials Interfaces* **2016**, *3*, 1500799.

(8) Fleischer, K.; Norton, E.; Mullarkey, D.; Caffrey, D.; Shvets, I. V. Quantifying the Performance of P-Type Transparent Conducting Oxides by Experimental Methods. *Materials* **2017**, *10*, 1019.

(9) Williamson, B. A. D.; Buckeridge, J.; Brown, J.; Ansbro, S.; Palgrave, R. G.; Scanlon, D. O. Engineering Valence Band Dispersion for High Mobility p-Type Semiconductors. *Chem. Mater.* **2017**, *29*, 2402−2413.

(10) Lunca-Popa, P.; Botsoa, J.; Bahri, M.; Crêpelliére, J.; Desgardin, P.; Audinot, J.-N.; Wirtz, T.; Arl, D.; Ersen, O.; Barthe, M.-F.; et al. Tuneable interplay between atomistic defects morphology and electrical properties of transparent p-type highly conductive off-stoichiometric Cu-Cr-O delafossite thin films. *Sci. Rep.* **2020**, *10*, 1416.

(11) Yokobori, T.; Okawa, M.; Konishi, K.; Takei, R.; Katayama, K.; Oozono, S.; Shinmura, T.; Okuda, T.; Wadati, H.; Sakai, E.; et al. Electronic structure of the hole-doped delafossite oxides CuCr$_{1-x}$Mg$_x$O$_2$. *Phys. Rev. B* **2013**, *87*, 195124.

(12) Norton, E.; Farrell, L.; Callaghan, S. D.; McGuinness, C.; Shvets, I. V.; Fleischer, K. X-ray spectroscopic studies of the electronic structure of chromium-based p-type transparent conducting oxides. *Phys. Rev. B* **2016**, *93*, 115302.

(13) Farrell, L.; Fleischer, K.; Caffrey, D.; Mullarkey, D.; Norton, E.; Shvets, I. V. Conducting mechanism in the epitaxial p-type transparent conducting oxide C r2 O3:Mg. *Phys. Rev. B* **2015**, *91*, 125202.

(14) Farrell, L.; Norton, E.; Smith, C. M.; Caffrey, D.; Shvets, I. V.; Fleischer, K. Synthesis of nanocrystalline Cu deficient CuCrO2-a high figure of merit p-type transparent semiconductor. *Journal of Materials Chemistry C* **2016**, *4*, 126−134.

(15) Farrell, L.; Norton, E.; O'dowd, B. J.; Caffrey, D.; Shvets, I. V.; Fleischer, K. Spray pyrolysis growth of a high figure of merit, nanocrystalline, p-type transparent conducting material at low temperature. *Appl. Phys. Lett.* **2015**, *107*, 031901.

(16) Sánchez-Alarcón, R. I.; Oropeza-Rosario, G.; Gutierrez-Villalobos, A.; Muro-López, M. A.; Martínez-Martínez, R.; Zaleta-Alejandre, E.; Falcony, C.; Alarcón-Flores, G.; Fragoso, R.; Hernández-Silva, O.; et al. Ultrasonic spray-pyrolyzed CuCrO2thin films. *J. Phys. D: Appl. Phys.* **2016**, *49*, 175102.

(17) Fredriksson, H.; Alaverdyan, Y.; Dmitriev, A.; Langhammer, C.; Sutherland, D. S.; Zäch, M.; Kasemo, B. Hole-Mask Colloidal Lithography. *Adv. Mater.* **2007**, *19*, 4297−4302.

(18) Levitsky, I.; Tavor, D. Improved Atomization via a Mechanical Atomizer with Optimal Geometric Parameters and an Air-Assisted Component. *Micromachines* **2020**, *11*, 584.

(19) Hallberg, C. J.; Lysaught, M. T.; Zmudka, C. E.; Kopesky, W. K.; Olson, L. E. Characterization of a human powered nebulizer compressor for resource poor settings. *BioMedical Engineering OnLine* **2014**, *13*, 77.

(20) Norton, E.; Farrell, L.; Zhussupbekova, A.; Mullarkey, D.; Caffrey, D.; Papanastasiou, D. T.; Oser, D.; Bellet, D.; Shvets, I. V.; Fleischer, K. Bending stability of Cu0.4CrO2—A transparent p-type conducting oxide for large area flexible electronics. *AIP Advances* **2018**, *8*, 085013.

(21) Hu, X.; Schuster, J.; Schulz, S. E.; Gessner, T. Surface chemistry of copper metal and copper oxide atomic layer deposition from copper(ii) acetylacetonate: a combined first-principles and reactive molecular dynamics study. *Phys. Chem. Chem. Phys.* **2015**, *17*, 26892−26902.

(22) Viguié, J. C.; Spitz, J. Chemical Vapor Deposition at Low Temperatures. *J. Electrochem. Soc.* **1975**, *122*, 585−588.

(23) Marchand, P.; Hassan, I. A.; Parkin, I. P.; Carmalt, C. J. Aerosol-assisted delivery of precursors for chemical vapour deposition: expanding the scope of CVD for materials fabrication. *Dalton Transactions* **2013**, *42*, 9406.

(24) Verre, R.; MacCaferri, N.; Fleischer, K.; Svedendahl, M.; Odebo Länk, N.; Dmitriev, A.; Vavassori, P.; Shvets, I. V.; Käll, M. Polarization conversion-based molecular sensing using anisotropic plasmonic metasurfaces. *Nanoscale* **2016**, *8*, 10576−10581.

(25) Caffrey, D.; Zhussupbekova, A.; Vijayaraghavan, R. K.; Ainabayev, A.; Kaisha, A.; Sugurbekova, G.; Shvets, I. V.; Fleischer, K. Crystallographic characterisation of ultra-thin, or amorphous transparent conducting oxides-the case for Raman spectroscopy. *Materials* **2020**, *13*, 267.

(26) Bajaj, J.; Irvine, S. J. C.; Sankur, H. O.; Svoronos, S. A. Modeling of in situ monitored laser reflectance during MOCVD growth of HgCdTe. *J. Electron. Mater.* **1993**, *22*, 899−906.

(27) Stafford, A.; Irvine, S. J. C.; Hess, K. L.; Bajaj, J. The use ofin situlaser interferometry for MOCVD process control. *Semicond. Sci. Technol.* **1998**, *13*, 1407−1411.

(28) Ng, T. B.; Han, J.; Biefeld, R. M.; Weckwerth, M. V. In-situ reflectance monitoring during MOCVD of AlGaN. *J. Electron. Mater.* **1998**, *27*, 190−195.

(29) Nakamura, S. Analysis of Real-Time Monitoring Using Interference Effects. *Jpn. J. Appl. Phys.* **1991**, *30*, 1348−1353.

(30) Verre, R.; Fleischer, K.; McGilp, J. F.; Fox, D.; Behan, G.; Zhang, H.; Shvets, I. V. Controlled in situ growth of tunable plasmonic self-assembled nanoparticle arrays. *Nanotechnology* **2012**, *23*, 035606.

(31) Verre, R.; Fleischer, K.; Sofin, R.; McAlinden, N.; McGilp, J.; Shvets, I. In situ characterization of one-dimensional plasmonic Ag nanocluster arrays. *Phys. Rev. B* **2011**, *83*, 125432.

(32) Plieth, W.; Naegele, K. Über die bestimmung der optischen konstanten dünnster oberflächenschichten und das problem der schichtdicke. *Surf. Sci.* **1977**, *64*, 484−496.

(33) Jellison, G. E.; Modine, F. A. Optical nature of interface layers: a comparative study of the Si−SiO_2 interface. *J. Opt. Soc. Am.* **1982**, *72*, 1253.

(34) Hu, J.; Wang, J.; Wei, Y.; Wu, Q.; Zhang, F.; Xu, Q. Effect of film growth thickness on the refractive index and crystallization of HfO2 film. *Ceram. Int.* **2021**, *47*, 33751−33757.

(35) Waechtler, T.; Roth, N.; Mothes, R.; Schulze, S.; Schulz, S. E.; Gessner, T.; Lang, H.; Hietschold, M. Copper Oxide ALD from a Cu(I) beta-Diketonate: Detailed Growth Studies on SiO2 and TaN. *ECS Trans.* **2009**, *25*, 277−287.

(36) von Hoene, J.; Charles, R. G.; Hickam, W. M. Thermal decomposition of metal acetylacetonates mass spectrometer studies. *J. Phys. Chem.* **1958**, *62*, 1098−1101.

(37) Lalancette, R. A.; Syzdek, D.; Grebowicz, J.; Arslan, E.; Bernal, I. The thermal decomposition and analyses of metal tris-acetylacetonates: Free radical formation from Al, Cr, Mn, Fe and Co complexes. *J. Therm. Anal. Calorim.* **2019**, *135*, 3463−3470.

(38) Tripathi, T. S.; Niemelä, J.-P.; Karppinen, M. Atomic layer deposition of transparent semiconducting oxide CuCrO2 thin films. *Journal of Materials Chemistry C* **2015**, *3*, 8364−8371.

(39) Chavez, K. L.; Hess, D. W. A Novel Method of Etching Copper Oxide Using Acetic Acid. *J. Electrochem. Soc.* **2001**, *148*, G640.

(40) Lee, S.-M.; Park, J.-H.; Hong, K.-S.; Cho, W.-J.; Kim, D.-L. The deposition behavior of SiO[sub 2]−TiO[sub 2] thin film by metalorganic chemical vapor deposition method. *Journal of Vacuum Science & Technology A: Vacuum, Surfaces, and Films* **2000**, *18*, 2384.

(41) Hodroj, A.; Deschanvres, J.-L.; Gottlieb, U. Growth of Amorphous Ti−Si−O Thin Films by Aerosol CVD Process at Atmospheric Pressure. *J. Electrochem. Soc.* **2008**, *155*, D110.

(42) Nasibulin, A. G.; Shurygina, L. I.; Kauppinen, E. I. Synthesis of nanoparticles using vapor-phase decomposition of copper(II) acetylacetonate. *Colloid J.* **2005**, *67*, 1−20.

(43) Han, M.; Wang, J.; Deng, Q.; Wang, J.; Li, W.; Zhang, P.; Li, C.; Hu, Z. Effect of annealing temperature on structural, optoelectronic properties and interband transitions of CuCrO2 nanocrystalline films prepared by the sol−gel method. *J. Alloys Compd.* **2015**, *647*, 1028−1034.

(44) Sander, T.; Reindl, C. T.; Giar, M.; Eifert, B.; Heinemann, M.; Heiliger, C.; Klar, P. J. Correlation of intrinsic point defects and the Raman modes of cuprous oxide. *Phys. Rev. B* **2014**, *90*, 045203.